Article

Characterization of Tungsten Sputtering Processes in a Capacitively Coupled Argon Plasma

Espedito Vassallo [1], Miriam Saleh [1,*], Matteo Pedroni [1], Anna Cremona [1] and Dario Ripamonti [2]

[1] Institute for Plasma Science and Technology (ISTP), National Research Council (CNR), Via R. Cozzi 53, 20125 Milan, Italy; espedito.vassallo@istp.cnr.it (E.V.); matteo.pedroni@istp.cnr.it (M.P.); anna.cremona@istp.cnr.it (A.C.)

[2] Institute of Condensed Matter Chemistry and Technologies for Energy (ICMATE), National Research Council (CNR), Via R. Cozzi 53, 20125 Milan, Italy; dario.ripamonti@cnr.it

* Correspondence: miriam.saleh@istp.cnr.it

Abstract: A capacitively coupled radio-frequency argon plasma, used for tungsten sputtering deposition, is characterized using Langmuir probe measurements. Druyvesteyn's method is used to evaluate plasma parameters through the integral of the Electron Energy Distribution Function (EEDF). In the pressure range analyzed (0.6–10 Pa), the obtained distributions are not Maxwellian, which suggests some depletion of electrons with higher energies. The obtained plasma parameters are compared with those derived from the graphical method. The electron temperature obtained via the graphical method is always lower than the effective temperatures derived from EEDFs, and vice versa, the electron density is overestimated by the graphical method. Optical Emission Spectroscopy is used to monitor the atoms sputtered in the plasma process. The behavior of excited species correlates with the plasma parameters.

Keywords: plasma sputtering; Langmuir probe; capacitively coupled argon plasma

Academic Editor: Andrey Starikovskiy

Received: 15 January 2025
Revised: 20 February 2025
Accepted: 26 February 2025
Published: 28 February 2025

Citation: Vassallo, E.; Saleh, M.; Pedroni, M.; Cremona, A.; Ripamonti, D. Characterization of Tungsten Sputtering Processes in a Capacitively Coupled Argon Plasma. *Plasma* **2025**, *8*, 8. https://doi.org/10.3390/plasma8010008

Copyright: © 2025 by the authors. Licensee MDPI, Basel, Switzerland. This article is an open access article distributed under the terms and conditions of the Creative Commons Attribution (CC BY) license (https://creativecommons.org/licenses/by/4.0/).

1. Introduction

Detailed information on plasma parameters is fundamental in magnetron sputtering systems for the industrial fabrication of coatings. These parameters include ion flux, electron temperature (T_e), electron density (n_e), plasma (V_s) and floating (V_f) potentials. The Langmuir probe (LP) is a proper tool to study these parameters because it directly measures key plasma characteristics. Its design allows for localized diagnostics, making it invaluable compared to more complex and expensive alternatives. It is commonly used in plasma diagnostics in both laboratory and industrial environments due to its simplicity and relatively low cost (compared to other diagnostic techniques such as laser-based diagnostics or interferometry) [1–3]. For example, in industrial settings, it enables monitoring of plasma parameters during large-scale coating processes, while in laboratories it provides essential data for research purposes without requiring advanced infrastructure. The LP is one of the oldest and most widely used tools for plasma diagnostics and consists of a small metallic electrode (or multiple electrodes) inserted into the plasma. A varying electric potential is applied between the probe tip and the processing chamber. The current flowing through the tip is measured as a function of the applied voltage to yield a current-voltage (I–V) curve. At high positive probe voltages (V_P), only electrons reach the probe. In contrast, only positive ions impinge on the probe tip at high negative V_P. In the intermediate voltage range, both electric charges can reach the probe depending on their energy distribution. By applying appropriate models to the different sections of the I–V characteristic, various

plasma discharge properties are derived (e.g., n_e, T_e, V_s, etc.). A limitation of LP is its use at high pressures in collisional or semi-collisional plasma regimes (especially in applications like plasma processing), where the frequency of collisions between particles (such as electrons and neutral atoms or ions) becomes comparable to the characteristic frequencies of the plasma [4]. In these regimes, electrons collide with neutral atoms or molecules, affecting their energy distribution and the overall energy dissipation in the plasma. These collisions influence how energy is transferred from the electric field to the particles. In these conditions, the classical analysis of I–V curves with the assumption that the plasma has a Maxwellian electron energy distribution function (EEDF) can complicate the interpretation of data, leading to inaccuracies (the software of commercial probes always assumes to have a Maxwellian EEDF). Many researchers [2,5,6] to determine plasma parameters have used the classical Langmuir probe analysis theories, including graphical techniques (a procedure where the n_e and the T_e are inferred from the electron part of the I–V characteristic), which are based on the main hypothesis that the EEDF is Maxwellian, but, as will be explained in this article, in a collisional or semi-collisional plasma this hypothesis is generally incorrect. It's crucial to remember that the EEDF plays a critical role in controlling ionization processes (but also excitation and dissociation processes), and understanding the EED can help improve the efficiency of these processes. In a collisional or semi-collisional plasma, the EEDF can deviate from a Maxwellian distribution due to the competing effects of collisions and external fields used in plasma generation. Electrons that do not collide frequently may gain higher energy from the fields, while those that collide often lose energy to neutrals, leading to a non-equilibrium distribution. Another type of distribution function exists, known as Druyvesteyn distribution [7,8]. The method is explained in the third paragraph. which allows the determination of the T_e and n_e through an integral of the EEDF

Druyvesteyn distribution has a reduced high-energy tail and more electrons with lower energy are expected.

In recent years, extensive experimental studies have been conducted to analyze the EEDF in low-pressure radiofrequency (RF) plasmas. While the majority of these investigations focus on plasma generation in inductively coupled plasma (ICP) sources [9–20], relatively fewer studies address capacitively coupled plasmas (CCPs). Notable research [21–24] has explored the effects of excitation frequency (ranging from 13 to 100 MHz) and power (ranging from 10 to 100 W) applied to the powered electrode on the EEDF in RF argon CCPs. This study examines Ar plasmas generated using a CCP source, with particular emphasis on how operating pressure (0.6–10 Pa) influences the EEDF. Plasma parameters are determined by an LP probe through the analysis of the I–V characteristics. The interpretation was performed by two different methods. The first is a method based on electron energy distribution function (EEDF) integrals, in which the T_e and n_e are determined from the integrals of the EEDF. The second one is based on the graphical technique (assuming a Maxwellian EEDF) in which the average T_e was determined as T_e (eV) = 1/slope of the plot of the natural logarithm of the I–V curve of the probe in the region between the V_f and V_P, while the n_e was calculated from the electron current saturation region [25,26]. Optical Emission Spectroscopy (OES) was also used to detect the characteristic wavelengths of the radiation emitted in the visible range by the sputtered atoms, correlating the line intensities to the plasma parameters. The morphological properties of the thick W films deposited on Si wafers were analyzed with a high-resolution Scanning Electron Microscope (SEM) and were related to the plasma process conditions.

2. Materials

2.1. Sputtering System

The experimental setup consisted of a capacitively coupled plasma (CCP) system in a magnetron sputtering configuration [27] (as shown in Figure 1). An RF supply was applied between two electrodes to create and sustain a plasma, with the distance between electrodes set at 0.06 m. The setup was housed in a cylindrical stainless-steel vacuum chamber with a volume of 0.04 m^3 (cylinder dimensions: diameter of 0.4 m and height of 0.5 m). The chamber was equipped with a balanced-type magnetron sputtering cathode, produced by Angstrom Sciences, Inc. The magnetic field within the system had a strength ranging from 50 to 100 Gauss. The cathode was water-cooled and connected to a separate RF ($\omega_{RF}/2\pi$ = 13.56 MHz) power supply (300 W, TRUMPF Hüttinger, Ditzingen, Germany), which operated in a steady state, coupled with an automatic impedance matching unit to minimize the reflected power. For optimal performance, a power setting of 75 W was chosen, striking a good balance between achieving an adequate deposition rate and maintaining an acceptable level of film stress.

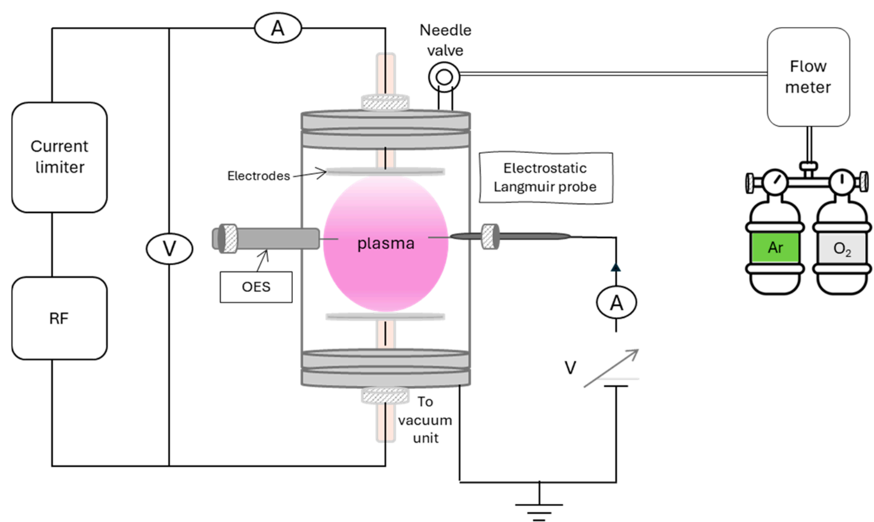

Figure 1. Schematic of the magnetron sputtering apparatus.

High-purity (99.9%) tungsten (W) target (size 3″, thickness 0.25″) was housed on the working powered electrode. The sputtering process was carried out in argon plasma at a constant flow rate of 20 SCCM (Standard Cubic Centimeters per Minute) under various pressure conditions. The working Ar flux and pressure were monitored by a mass flow controller (MKS) and a vacuum gauge (Pfeiffer single Gauge, Aßlar, Germany), respectively. The sputtering chamber evacuation system consisted of a backing pump to pre-evacuate the chamber (TRIVAC 24 m^3/h, Leybold, Cologne, Germany) in combination with a turbo-molecular pump (TURBOVAC 150 l/s, Leybold, Cologne, Germany) to ensure efficient evacuation (base pressure of 1×10^{-4} Pa). The W films were deposited on silicon wafers (10×10 mm^2, 400 µm thick) placed on the ground electrode. Regarding the W coating characterization, high-resolution scanning electron microscope (Hi-res SEM, Tescan mod. MIRA III, Brno, Czech Republic) imaging was used to evaluate the morphology of films. The deposition rate (*DR*) was estimated by dividing the film thickness (calculated by a P15 surface profiler KLA Tencor, Milpitas, California, CA USA) by the deposition time. The density of the W coatings (ρ) was estimated by weighing the Si wafer before and after the W deposition (Δm) on a balance accurate at least to the nearest 10^{-5} g (Model Sartorius SECURA225D-1S, Gottingen, Germany). As the coating thickness (d) was known, the coating density was found from the formula: $\rho = \Delta m/d{\cdot}A$ (A = Si wafer area).

2.2. Langmuir Probe Set-Up

A Hiden's ESPION RF-compensated Langmuir probe system (Warrington, UK) was used to measure the I–V characteristics during the sputtering process. The cylindrical probe tip (tungsten wire, diameter = 0.15 mm, length = 10 mm) was inserted into the vacuum chamber at the center of the discharge (parallel to the electrodes) at a fixed position (2.5 cm below the powered electrode. The probe had 13.56 MHz and 27.12 MHz resonance filters and a reference ring to avoid RF distortion [28]. The probe collected electrons and ions, measuring the current collected by applying a bias voltage, which varied from −60 V to 60 V in steps of 1 V. Since the probe tip can accumulate a layer of material from the plasma (distorting the I–V characteristics), it was cleaned by applying a −20 V potential for a period of 95 ms before each data acquisition. Moreover, the obtained I–V curve came from an average of five scans.

2.3. Optical Emission Spectroscopy Set-Up

Plasma was characterized by Optical Emission Spectroscopy (OES). The spectrometer consisted of a scanning monochromator (Horiba Jobin Yvon iHR550, Palaiseau, France) of the Czerny–Turner type (focal length = 0.55 m), equipped with a holographic diffraction grating with 1800 grooves/mm, coupled to a CCD (Synapse Horiba Jobin Yvon, Palaiseau, France) camera. Light from the plasma was gathered using a 1″ diameter plane-convex lens and an optical fiber and focused onto the entrance slit of the monochromator. The spectral resolution of the instrument was 0.06 nm and the wavelength accuracy was 0.2 nm. The spectroscopic measurements were taken along a line of sight about 3 cm from the substrate on the ground electrode.

3. Langmuir Probe Measurement Method

In sputtering processes, non-equilibrium plasmas are typically encountered. A key limitation of many conventional Langmuir probe theories used for plasma diagnostics is the assumption that electrons follow a Maxwellian Electron Energy Distribution Function (EEDF). In real scenarios, this condition is rarely met, and relying on this assumption can result in significant errors in determining plasma parameters. For non-Maxwellian plasmas, Druyvesteyn's method proves particularly useful; it does not simply derive the n_e from the T_e and the probe saturation current [29]. Druyvesteyn's method directly calculates electron density regardless of the EEDF's shape. This is achieved through an integral of the EEDF, which is derived by performing a double differentiation of the I–V curve of a cylindrical probe in the electron retardation range [30]. The $f(\varepsilon)$ = EEDF is determined by the Druyvesteyn equation [31,32] as follows:

$$f(\varepsilon) = \frac{4}{Ae^2}\sqrt{\frac{m\varepsilon}{2e}}\frac{d^2I}{dV^2} \quad (1)$$

where $\varepsilon = e\,(V_s - V)$ is the electron energy, A is the surface area of the probe exposed to the plasma, I is the electron retarding current collected by the probe, e and m are the electron charge and mass, respectively. V_s is the plasma potential and V is the applied bias voltage to the probe. V_s is estimated by finding the zero crossing of the second derivative of the current-voltage (I–V) characteristic curve. According to Druyvesteyn's method, the n_e can be calculated by numerical integration of the EEDF:

$$n_e = \int_0^\infty f(\varepsilon)d\varepsilon \quad (2)$$

For non-Maxwellian EEDF, the T_e is called the effective electron temperature (T_{eff}), which corresponds to the average electron energy [33] and can be calculated by the equation:

$$T_{eff} = \frac{2 < \varepsilon >}{3} = \frac{2}{3\, n_e} \int_0^{\infty} \varepsilon f(\varepsilon)\, d\varepsilon \quad (3)$$

4. Results and Discussion

The electron energy distribution functions (EEDFs) of an Ar plasma (obtained from the I–V characteristics of the probe by means of Druyvesteyn's method) as a function of pressure are shown in Figure 2a at an RF power of 75 W. It is noted that at low pressure, the EEDF closely follows a bi-Maxwellian distribution. As the pressure increases (≥2 Pa), the EEDF shape gradually changes, and it starts resembling a Druyvesteyn distribution. This transition suggests a shift in the plasma dynamics, where the electron collisions become more frequent. The comparison of the experimentally determined EEDF at a pressure of 1 Pa (RF power of 75 W) with a Maxwellian distribution is shown in Figure 2b. As expected, the experimental distribution decreases more sharply than the Maxwellian for energies above 20 eV. This suggests that high-energy electrons are less frequent than predicted by a Maxwellian distribution, likely due to inelastic collisions in the plasma. The results challenge the assumption of a Maxwellian electron energy distribution, especially in magnetron discharges [34]. In such discharges, due to the complex interactions between electrons and heavy particles, the EEDF often deviates from Maxwellian. This is particularly true at higher energies and in the presence of complex plasma dynamics like those found in magnetron discharges. As demonstrated by scientific literature [35], both stochastic and ohmic heating occur simultaneously in capacitively coupled plasma (CCP). At the pressure of 2 Pa, the electron mean free path $(\lambda_{e,\,mfp})$, estimated using the total cross sections [36] and the gas pressure, is approximately 2 cm (as shown in Figure 3). This value is much smaller than the distance between the electrodes, meaning that at this pressure, the plasma becomes decidedly more collisional, leading to an increase in ohmic heating. It is important to note that the $\lambda_{e,\,mfp}$ is significantly longer than that of the ions (as the ion-neutral collision cross-section, we used a value of $\approx 8 \times 10^{-19}$ m^2 [37]) due to the smaller size of the electrons, which results in a greater probability of collisions for ions compared to electrons in this plasma environment. At higher pressures, the frequency and energy of collisions between electrons and heavy particles (such as atoms, ions, and neutrals) in a plasma environment increase (inelastic excitation and ionization processes [38]), the high-energy tail of the EEDF decreases, and the number of lower-energy electrons increases, resulting in changes in the shape of the EEDFs due to the electron energy loss, and therefore effective electron temperature drops (Figure 4).

The T_e and n_e were measured using the graphical and EEDF integral methods. Figure 4 presents the experimental results for the T_e and n_e measurements as a function of pressure under a constant input power of 75 W. A comparison of the results shows that the values obtained from the graphical method exhibit poor agreement with those derived from EEDF analysis. Specifically, the T_e calculated from the EEDF data is consistently higher than the T_e found from the graphical method. This discrepancy is particularly noticeable at lower pressures, where the EEDF shape becomes more complex (Figure 2a), deviating from bi-Maxwellian to Druyvesteyn distribution. A similar trend is observed for the n_e, where the graphical method tends to overestimate it. This overestimation is attributed to the assumption in the graphical method that n_e is inversely proportional to the square root of T_e [39].

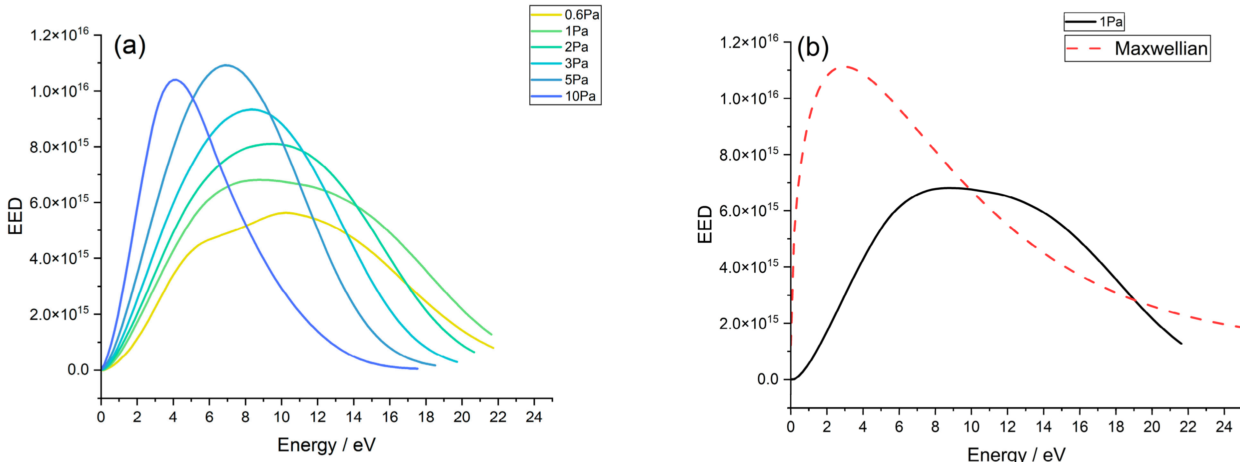

Figure 2. (**a**) Electron energy probability functions (EEDs) as a function of pressure at 75 W input power. (**b**) Comparison between Maxwell's distribution and the experimental one at 1 Pa.

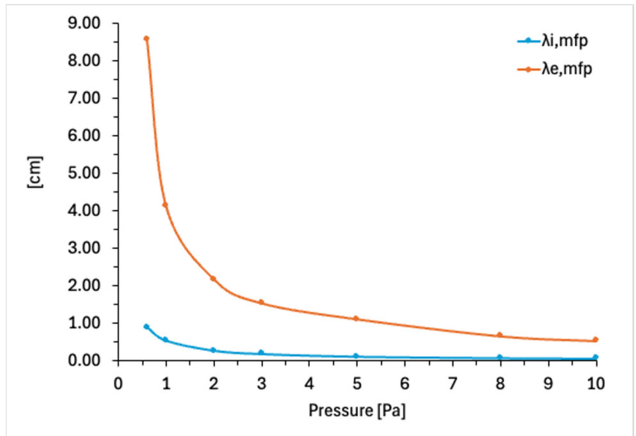

Figure 3. The estimated value of ion and electrons mean free path (mfp) at various pressures and power of 75 W.

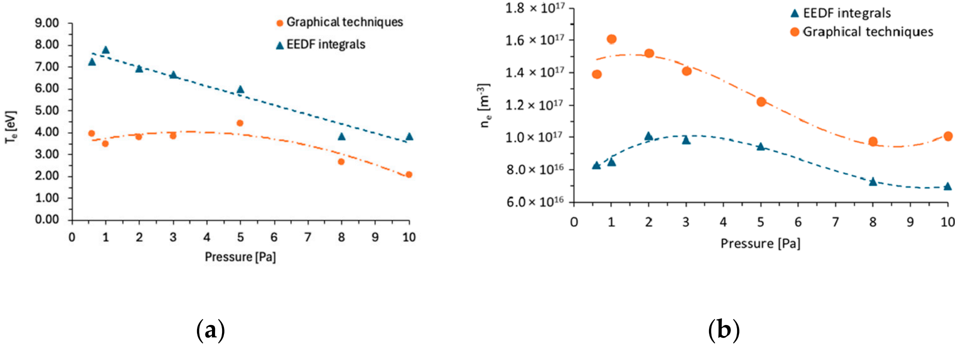

(**a**) (**b**)

Figure 4. (**a**) T_e and (**b**) n_e obtained by the graphical and EEDF integral methods, which were generated by various pressures at 75 W input power.

Regarding the trend of n_e, it was observed to increase with pressure in the low-pressure range. This increment can primarily be attributed to an enhanced ionization frequency, where the rate of ionization rises as pressure increases. However, n_e reaches a maximum at approximately 2–3 Pa and then begins to decrease as pressure continues to rise. This trend is determined by the fact that at high pressures, electrons lose energy more quickly, leading to a reduction in n_e and, consequently, plasma density. This happens because the $\lambda_{e,\,mfp}$ is strongly reduced at higher pressures due to the more frequent collisions

between electrons and neutral gas atoms, causing energy loss and reducing the number of electrons. In addition, electron thermalization is generated. This results in a lower density of high-energy electrons, as confirmed by the change in EEDF form (Figure 2). Higher pressures also enhance diffusion effects, where electrons diffuse out of the plasma region, further lowering the overall electron density.

Simultaneously, the reduction in T_e with increasing pressure can be attributed to an increase in the frequency of inelastic electron-heavy particle collisions, which leads to a cooling effect [40]. As pressure rises, the electron mean free path decreases (as shown in Figure 3), resulting in more frequent energy exchanges between the electrons and gas particles. This enhanced energy transfer contributes to the reduction of T_e. The observed trends are consistent with other experimental results, supporting the validity of these findings in similar plasma conditions [41–44].

The electric space potential of the plasma, often referred to as the plasma potential (V_s), is one of the most important parameters. It plays a crucial role in determining the behavior of charged particles within the plasma and the surrounding region. The V_s was determined from the zero-crossing voltage of the second derivative of the current and from the I–V characteristics using the intersecting slopes technique [45]. It was observed that the V_s value determined by the graphical technique is slightly higher than that determined by Druyvesteyn's method. For clarity, only the values obtained using Druyvesteyn's method are presented in Figure 5. Additionally, the variation of both V_s and floating potential V_f (defined as the potential assumed by a probe when the fluxes of electrons and ions impinging on the probe are equal, resulting in zero net current flowing through the probe) as a function of sputtering pressure at an RF power of 75 W was analyzed. This analysis provides insights into the relationship between these potentials and the sputtering pressure under the given experimental conditions. As pressure increased, the V_s decreased from 26.5 V at 0.5 Pa to 18.5 V at 10 Pa, while the V_f remained almost constant with a slight decrease. The difference between V_s and V_f serves as an indicator of the energy of the charged particles bombarding the substrate, as described in reference [46]. These charged particles strike the substrate with varying energies, which, along with the flux, influences the growth of the coating and the structural features that develop on the substrate's surface. In this study, the $V_s - V_f$ difference decreased as pressure increased, which is attributed to the decrease in V_s influenced by high-energy electrons [21,47]. These high-energy electrons decreased as pressure rose, as seen in Figure 2, leading to a subsequent reduction in the T_e shown in Figure 4.

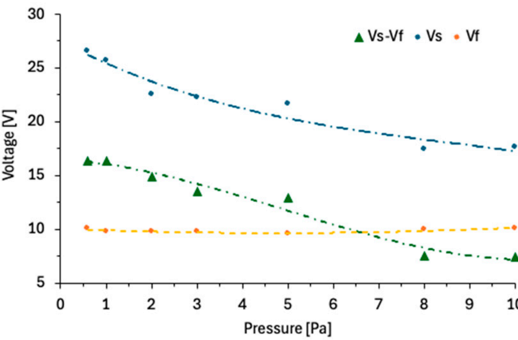

Figure 5. Pressure dependence of V_s and V_f at RF power of 75 W.

Under our experimental conditions, $V_s - V_f$ was only weakly affected by pressure, varying from 16 V to 7 V across the pressure range. Consequently, this weak dependence indicates that pressure does not significantly impact the morphological structure of the coatings [21]. However, as we will demonstrate later, pressure has a pronounced effect

on other coating characteristics. Specifically, pressure variations strongly influence the ion energy distribution [48], ion density (evaluated via the Bohm criterion [49]), and ion flux (Γ_i) reaching the target. These factors affect the target sputtering rate (SR), which is challenging to determine directly due to complex angular distributions and re-deposition effects. While SR is difficult to measure directly, it influences the flux of atoms arriving at the substrate, which is what we effectively measure and ultimately determines the deposition rate (DR). Using the n_e values obtained from Druyvesteyn's method, as one might expect according to the n_e trend (Figure 4), the behavior of Γ_i as a function of pressure exhibits a bell-shaped curve, with a peak at approximately 2–3 Pa (Figure 6). The DR increases with pressure, reaching a maximum at 5 Pa, and then decreases as pressure continues to rise.

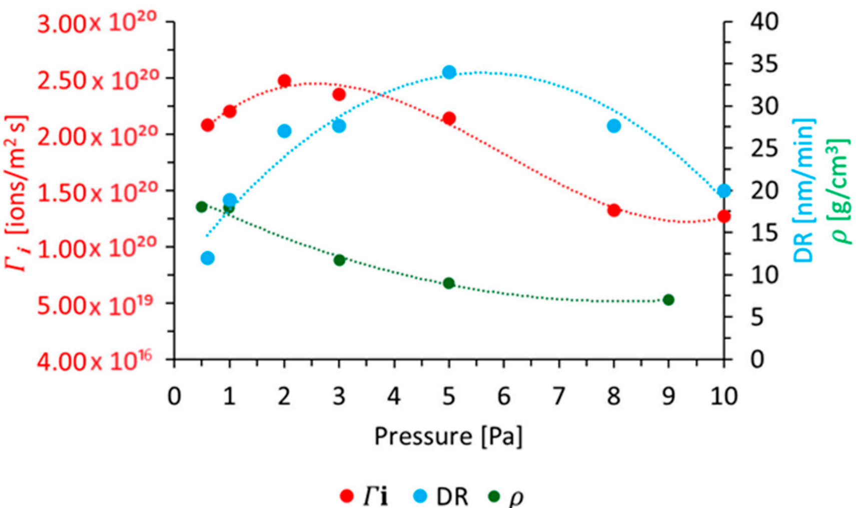

Figure 6. Γ_i, DR and W coating density as a function of the pressure.

The target SR depends on the balance between ion flux and mean ion energy, but since the negative bias at the rf-powered electrode (V_{dc}, also referred to as the DC-bias or self-bias voltage [50]) varies only slightly within the pressure range of 0.5–10 Pa (ranging from 420 to 390 V), the sputtering rate is primarily influenced by ion flux. The ion flux increases up to 2–3 Pa, resulting in a greater number of sputtered atoms and, consequently, an increase in the DR at a fixed power. Beyond this pressure range, further increases in pressure lead to a higher particle density but also an increase in ion and electron collision frequency, as evidenced by the trends in ionic and electronic mean free paths (Figure 3). These collisions enhance volume recombination processes, which reduce the ion flux and, consequently, the SR. Additionally, increased scattering of both ions (contributing to the reduced SR) and sputtered atoms occurs at higher pressures, explaining the observed decrease in the DR above a certain pressure threshold.

Moreover, with increasing pressure in a sputtering process, the mean free path of the sputtered atoms decreases, which results in a lower kinetic energy when they reach the substrate surface. This reduction in energy limits the mobility of the adatoms (adsorbed atoms) on the surface. As a consequence, these adatoms have less ability to rearrange and diffuse to form a densely packed, uniform coating. This can lead to a lower density of the deposited material on the substrate surface (Figure 6).

The influence of plasma parameters on the structural and morphological properties of the W-deposited coatings has been analyzed using SEM diagnostics (Figure 7). The microstructure, including morphology and porosity, is affected by the deposition pressure through plasma parameters such as electron density and electron temperature. Within the studied pressure range, deposition conditions generally promote the formation of columnar structures. These observations can be interpreted within the framework of structure zone

models, such as those developed by Movchan and Demchisin and Thornton [51,52]. These models relate the coating microstructure to the substrate temperature (T) normalized to the melting point of the coating material (Tm) and, in the case of the Thornton model, the argon pressure. In our experiments, the substrate temperature was not actively controlled and remained relatively low. Given these conditions, our coatings primarily fall within Zone 1 of these models, where limited adatom mobility leads to the formation of porous columnar structures. However, the greater density observed at lower pressures (Figure 7b) suggests that decreasing the pressure is promoting more Zone T-like behavior. At lower pressures, sputtered atoms undergo fewer gas-phase collisions and arrive at the substrate with increased kinetic energy. This higher energy effectively enhances adatom mobility, allowing for some degree of surface diffusion and a more compact microstructure. This is consistent with the Thornton model, where decreasing the argon pressure shifts the microstructure towards a denser structure, even at relatively low substrate temperatures. The cross-section SEM image of W coatings deposited at a pressure of 5 Pa (Figure 7a) reveals thin columns oriented perpendicular to the substrate surface, with visible voids and defects, indicative of a less dense Zone 1 microstructure. At lower pressures (Figure 7b), the columnar structure is partly maintained, but the reduced porosity and increased density, as confirmed by the measurement of coating density (Figure 6), suggest a shift towards a more compact microstructure. This increased density can be attributed to the combined effects of the increased mean free path and higher adatom kinetic energy at lower pressures. Moreover, no ions were detected along the line of sight considered, because ions are concentrated near the RF electrode. With fewer collisions before reaching the substrate, the atoms travel more freely and possess higher surface mobility, facilitating the formation of denser and smoother coatings, while remaining neutral in greater quantities than ions.

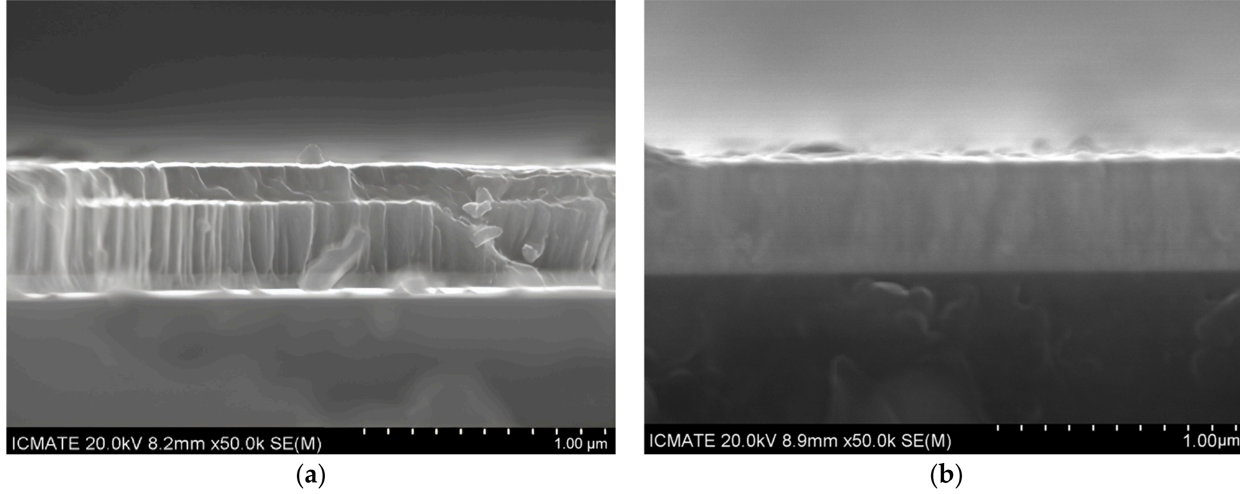

Figure 7. Cross-section SEM images of the deposited W coatings at the pressure of 5 Pa (**a**) and 1 Pa (**b**) at a fixed power of 75 W.

The plasma generated during the sputtering of the W target was investigated by optical emission spectroscopy analysis. Neutral atomic species were identified: Ar I and W I. Figure 8 shows an optical spectrum in the representative wavelength range 380–435 nm. No ions were detected along the line of sight considered, because Ar ions are concentrated near the RF electrode and the ionization mean free path of W atoms, sputtered as neutral, is too long compared to the vessel size. The intensity of Ar I spectral lines (750.39 nm, 751.47 nm, 763.51 nm) obtained from the acquired spectra and plotted vs. pressure (Figure 9) is consistent with the behavior of the incident ion flux Γ_i (Figure 6) and the electronic density n_e (Figure 4b) calculated by EEDF integrals: where Γ_i and n_e are

increasing, neutral Ar lines are decreasing and vice versa, with the dominant species in the plasma remaining neutral. The higher growth of the 750.39 nm line intensity is ascribable to the atomic data, particularly the shape of the electron-impact excitation cross section. The experimental trend of Ar I emission lines vs. pressure supports the results obtained by Langmuir probe measurements and corroborates the accuracy of the analysis method of the I–V characteristics based on EEDF integrals. Figure 10 shows the intensity of three emission W I lines (400.88 nm, 429.46 nm and 498.26 nm) as a function of pressure: the intensity of all the lines increases in the 1–3 Pa pressure range and decreases at pressures higher than 3 Pa, following the same behavior of the ion flux Γ_i (Figure 6) and the electron density n_e, estimated by EEDF integrals (Figure 4b). At pressures lower than 3 Pa the increase of the line intensities suggests that the W emission intensity is governed mainly by the increase of the incident ion flux Γ_i generating more sputtered atoms rather than by the decrease of the temperature of electrons responsible for the excitation of W atoms. Therefore, the intensity of W spectral lines can be considered representative of the density of sputtered atoms and related to the coating deposition on the target.

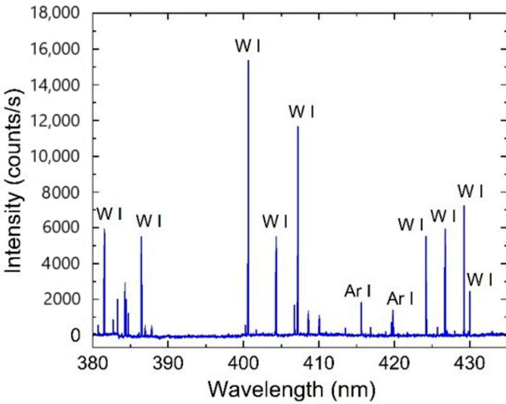

Figure 8. Optical spectrum in the 380–435 nm wavelength range.

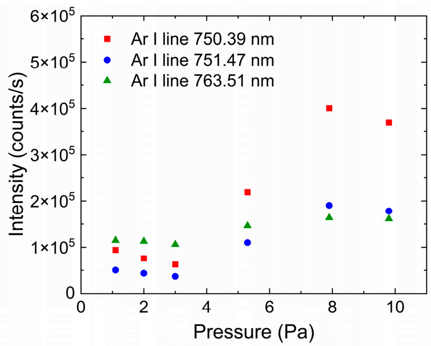

Figure 9. Ar I experimental line emission intensities vs. pressure.

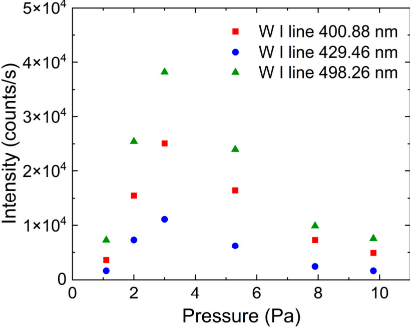

Figure 10. W I experimental line emission intensities vs. pressure.

5. Conclusions

In order to have a good understanding of the properties and dynamics of the plasma in a planar RF magnetron sputtering system, a Langmuir probe was used to measure the current-voltage characteristics of plasma, providing valuable data about n_e, T_e, V_s and Γ_i, while Optical Emission Spectroscopy was used to analyze the light emitted from excited species in the plasma to provide information about the plasma composition.

Plasma plays a critical role in providing energy to the species involved in sputtering processes, influencing key parameters that determine the quality, structure and properties of the deposited films. Tungsten thin films were produced at various process pressures, and the plasma discharge characteristics were correlated with the coating characteristics.

Two methods were employed to analyze the I–V characteristics: the graphical method, which follows the standard analysis procedure based on the assumption of a Maxwellian Electron Energy Distribution Function (EEDF), and Druyvesteyn's method, which accounts for deviations from the Maxwellian shape, as commonly observed in magnetron sputtering systems.

Both methods showed similar trends for T_e and n_e. The decrease in T_e with increasing pressure can be attributed to enhanced inelastic electron-heavy particle collisions (cooling effect), while the reduction in n_e is primarily due to volume recombination processes. However, significant discrepancies between the results of the two methods highlight the limitations of the standard graphical method, as it relies on the incorrect assumption of a Maxwellian EEDF. Consequently, Druyvesteyn's method emerges as the more reliable approach for measuring plasma parameters in Langmuir probe diagnostics.

SEM cross-sectional images of the microstructure revealed that the coatings exhibit a columnar structure. At lower pressures, the structure becomes denser and more compact due to the increased mean free path of sputtered atoms, enabling them to reach the substrate with higher energy.

Optical Emission Spectroscopy shows that the intensity of W spectral lines is consistent with the pressure behavior of Γ_i and n_e, estimated by EEDF integrals, and can be considered representative of the density of sputtered atoms and related to the coating deposition on the target.

Author Contributions: Conceptualization, M.S., M.P. and A.C.; investigation, E.V., M.S., M.P., A.C. and D.R.; data curation, M.S., M.P., A.C. and D.R.; writing—original draft preparation, E.V.; writing—review and editing, E.V., M.S., M.P., A.C. and D.R.; project administration, E.V. All authors have read and agreed to the published version of the manuscript.

Funding: This research received no external funding.

Institutional Review Board Statement: Not applicable.

Informed Consent Statement: Not applicable.

Data Availability Statement: The original contributions presented in this study are included in the article material. Further inquiries can be directed to the corresponding author.

Conflicts of Interest: The authors declare no conflicts of interest.

References

1. Cherrington, B.E. The use of electrostatic probes for plasma diagnostics. *Plasma Chem. Plasma Process.* **1982**, *2*, 113. [CrossRef]
2. Merlino, R.L. Understanding Langmuir probe current-voltage characteristics. *Am. J. Phys.* **2007**, *75*, 1078. [CrossRef]
3. Knappmiller, S.; Robertson, S.; Sternovsky, Z. Method to find the electron distribution function from cylindrical probe data. *Phys. Rev. E* **2006**, *73*, 066402. [CrossRef]
4. Kortshagen, U.; Schluter, H.J. Surface-wave propagation in homogeneous. *Phys. D Appl. Phys.* **1992**, *25*, 644. [CrossRef]

5. Lindner, J.; Ross, U.; Roddatis, V.; Jooss, C. Langmuir analysis of electron beam induced plasma in environmental TEM. *Ultramicroscopy* **2023**, *243*, 113629. [CrossRef]
6. Ohtsu, Y.; Fujita, H. Production of high-density capacitive plasma by the effects of multihollow cathode discharge and high-secondary-electron emission. *Appl. Phys. Lett.* **2008**, *92*, 171501. [CrossRef]
7. Druyvesteyn, M.J.; Penning, F.M. The Mechanism of Electrical Discharges in Gases of Low Pressure. *Rev. Mod. Phys.* **1940**, *12*, 87. [CrossRef]
8. Fullarton Boyd, R.L.; Twiddy, N.D. Pressure broadening studies on vibration-rotation bands II. *The effective collision diameters. Proc. R. Soc. A* **1959**, *250*, 53.
9. Chung, T.H.; Shin, Y.M.; Seo, D.C. Comparison of two methods of interpretation of Langmuir probe data for an inductively coupled oxygen plasma. *Contrib. Plasma Phys.* **2006**, *46*, 348. [CrossRef]
10. Sahu, B.B.; Han, J.G.; Kim, J.B.; Kumar, M.; Jin, S.; Hori, M. Study of Plasma Properties for the Low-Temperature Deposition of Highly Conductive Aluminum Doped ZnO Film Using ICP Assisted DC Magnetron Sputtering. *Plasma Process. Polym.* **2016**, *13*, 134. [CrossRef]
11. Sasaki, T.; Takahashi, K.; Fujiwara, T.J. Electron Energy Distributions in a Radiofrequency Plasma Expanded by Permanent Magnets. *Plasma Fusion Res. SERIES* **2010**, *9*, 422.
12. Kim, J.Y.; Kim, Y.-C.; Kim, Y.-S.; Chung, C.-W. Effect of the electron energy distribution on total energy loss with argon in inductively coupled plasma. *Phys. Plasmas* **2015**, *22*, 013501. [CrossRef]
13. Yang, W.; Wang, Y.-N. Fundamental study towards a better understanding of low pressure plasma etching. *Plasma Phys. Control. Fusion* **2021**, *63*, 035031. [CrossRef]
14. Chung, C.W. Experimental investigation on the floating potential of cylindrical Langmuir probes in non-Maxwellian electron distributions. *Phys. Plasmas* **2005**, *12*, 123505.
15. Roh, H.-J.; Kim, N.-K.; Ryu, S.; Park, S.; Lee, S.-H.; Huh, S.-R.; Kim, G.-H. Determination of electron energy probability function in low-temperature plasmas from current—Voltage characteristics of two Langmuir probes filtered by Savitzky–Golay and Blackman window methods. *Curr. Appl. Phys.* **2015**, *15*, 1173.
16. Lee, H.-C.; Seo, B.H.; Kwon, D.-C.; Kim, J.H.; Seong, D.J.; Oh, S.J.; Chung, C.W.; You, K.H.; Shin, C.H. Evolution of electron temperature in inductively coupled plasma. *Appl. Phys. Lett.* **2017**, *110*, 014106. [CrossRef]
17. Okada, K.; Komatsu, S.; Matsumoto, S.J. Langmuir probe measurements in a low pressure inductively coupled plasma used for diamond deposition. *Vac. Sci. Technol. A* **1999**, *17*, 721.
18. Lee, Y.-K.; Hwang, K.-T.; Lee, M.-H.; Chung, C.-W. Measurement of plasma parameters in an inductively coupled plasma using a double Langmuir probe. *J. Korean Phys. Soc.* **2008**, *52*, 1792. [CrossRef]
19. Chung, T.H.; Lee, Y.W.; Joh, H.M.; Song, M.A. Pressure dependence of dissociation fraction and optical emission characteristics in low-pressure inductively coupled N2-Ar plasmas. *AIP Adv.* **2011**, *1*, 032136. [CrossRef]
20. Choi, I.; Chung, C.W.; Moon, S.Y. Electron density and electron temperature measurement in a bi-Maxwellian electron distribution using a derivative method of Langmuir probes. *Phys. Plasmas* **2013**, *20*, 083508. [CrossRef]
21. Yin, G.; Gao, S.; Liu, Z.; Yuan, Q. The discharge characteristics of low-pressure capacitively coupled argon plasma with Langmuir probe. *Phys. Lett. A* **2022**, *426*, 127910. [CrossRef]
22. Azooz, A.A.; Ali, Z.T. Two Temperatures Components in CCP Argon 13.56-MHz RF Discharge. *IEEE Trans. Plasma Sci.* **2015**, *43*, 1774. [CrossRef]
23. Ahn, S.K.; You, S.J.; Chang, H.Y. Driving frequency effect on the electron energy distribution function in capacitive discharge under constant discharge power condition. *Appl. Phys. Lett.* **2006**, *89*, 161506. [CrossRef]
24. Zhu, X.M.; Chen, W.C.; Zhang, S.; Guo, Z.G.; Hu, D.W.; Pu, Y.K. Electron density and ion energy dependence on driving frequency in capacitively coupled argon plasmas. *J. Phys. D Appl. Phys.* **2007**, *40*, 7019. [CrossRef]
25. Chen, F.F. *Plasma Diagnostic Techniques*; Huddlestone, R.H., Leonard, S.L., Eds.; Academic Press: Cambridge, MA, USA, 1965; p. 113.
26. Heidenreich, J.E.; Paraszczak, J.R.; Moisan, M.; Sauve, G.J. Electrostatic probe analysis of microwave plasmas used for polymer etching. *Vac. Sci. Technol. B Microelectron. Nanometer Struct.* **1987**, *5*, 347. [CrossRef]
27. Kelly, P.J.; Arnell, R.D. Magnetron sputtering: A review of recent developments and applications. *Vacuum* **2000**, *56*, 159. [CrossRef]
28. Godyak, V.J. RF discharge diagnostics: Some problems and their resolution. *Appl. Phys.* **2021**, *129*, 041101. [CrossRef]
29. Hershkowitz, N. *Plasma Diagnostics, Discharge Parameters and Chemistry*; Auciello, O., Flamm, D.L., Eds.; Academic Press: Cambridge, MA, USA, 1989; ISBN 978-0-12-067635-4.
30. Sudit, I.D.; Woods, R.C. A workstation based Langmuir probe system for low-pressure dc plasmas. *Rev. Sci. Instrum.* **1993**, *64*, 2440. [CrossRef]
31. Druyvesteyn, M.J. Der Niedervoltbogen. *Z. Phys.* **1930**, *64*, 781.
32. Lieberman, M.A.; Lichtenberg, A.J. *Principles of Plasma Discharges and Materials Processing*, 2nd ed.; Wiley: Hoboken, NJ, USA, 2005; Chapter 18; ISBN 978-0-471-72001-0.

33. Abdel-Fattah, E.; Sugai, H. Combined effects of gas pressure and exciting frequency on electron energy distribution functions in hydrogen capacitively coupled plasmas. *Phys. Plasmas* **2013**, *20*, 023501. [CrossRef]
34. Ivanov, I.; Statev, S.; Orlinov, V.; Shkevov, R. Electron energy distribution function in a dc magnetron sputtering discharge. *Vacuum* **1992**, *43*, 837. [CrossRef]
35. Turner, M.M. Collisionless heating in radio-frequency discharges: A review. *J. Phys. D Appl. Phys.* **2009**, *42*, 194008. [CrossRef]
36. Ferch, J.; Granitza, B.; Masche, C.; Raith, W. Electron-argon total cross section measurements at low energies by time-of-flight spectroscopy. *J. Phys. B Atom. Mol. Phys.* **1985**, *18*, 967. [CrossRef]
37. Phelps, A.V. The application of scattering cross sections to ion flux models in discharge sheaths. *J. Appl. Phys.* **1994**, *76*, 747.
38. Singh, H.; Graves, D.B. Measurements of the electron energy distribution function in molecular gases in a shielded inductively coupled plasma. *J. Appl. Phys.* **2000**, *87*, 4098. [CrossRef]
39. Jauberteau, J.L.; Jauberteau, I. Plasma parameters deduced from cylindrical probe measurements: Determination of the electron density at the ion saturation current. *Plasma Sources Sci. Technol.* **2008**, *17*, 015019. [CrossRef]
40. Lieberman, M.A.; Lichtenberg, A.J. *Principles of Plasma Discharges and Materials Processing*, 2nd ed.; Wiley: Hoboken, NJ, USA, 2005; Chapter 3; ISBN 978-0-471-72001-0.
41. Chu, P.K.; Qin, S.; Chan, C.; Cheung, N.W.; Ko, P.K. Instrumental and process considerations for the fabrication of silicon-on-insulators (SOI) structures by plasma immersion ion implantation. *IEEE Trans. Plasma Sci.* **1998**, *26*, 79. [CrossRef]
42. Wu, S.Z. Pressure-Induced Anomalous Phase Transitions and Colossal Enhancement of Piezoelectricity in PbTiO3. *J. Appl. Phys.* **2005**, *98*, 083301. [CrossRef]
43. Hwang, K.; Oh, S.; Choi, I.; Chung, C. Measurement of electron temperature and ion density using the self-bias effect in plasmas. *Phys. Plasmas* **2010**, *17*, 063501. [CrossRef]
44. Sackers, M.; Busch, C.; Tsankov, V.; Czarnetzki, U.; Mertens, P.; Marchuk, O. Plasma parameters and tungsten sputter rates in a high-frequency CCP. *Phys. Plasmas* **2022**, *29*, 043511. [CrossRef]
45. Abdel-Fattah, E. Investigation of capacitively coupled argon plasma driven at various frequencies and validation of surface waves excitation. *Phys. Lett. A* **2013**, *377*, 297. [CrossRef]
46. Kumari, N.; Das, P.S.; Joshi, N.K.; Barhai, P.K. Correlations of plasma parameters and properties of magnetron sputtered TiN films. *Eur. Phys. J. Appl. Phys.* **2012**, *59*, 20302. [CrossRef]
47. Takenaka, K.; Setsuhara, Y.; Nishisaka, K.; Ebe, A. Meters-Scale Large-Area Plasma Sources with Multiple Low-Inductance Antenna Units for Next-Generation Flat-Panel Display Processing. *Trans. Mater. Res. Soc. Jpn.* **2007**, *32*, 493. [CrossRef]
48. Mirzaei, S.; Alishahi, M.; Souček, P.; Buršíková, V.; Zábranský, L.; Gröner, L.; Burmeister, F.; Blug, B.; Daum, P.; Mikšová, R.; et al. Effect of substrate bias voltage on the composition, microstructure and mechanical properties of W-B-C coatings. *Appl. Surf. Sci.* **2020**, *528*, 146966. [CrossRef]
49. Kusano, E.; Fukushima, K.; Saitoh, T.; Saiki, S.; Kikuchi, N.; Nanto, H.; Kinbara, A. Effects of Ar pressure on ion flux energy distribution and ion fraction in r.f.-plasma-assisted magnetron sputtering. *Surf. Coat. Technol.* **1999**, *120–121*, 189. [CrossRef]
50. Jiang, W.; Wang, H.; Bi, Z.; Wang, Y. Effects of Ar pressure on ion flux energy distribution and ion fraction in r.f.-plasma-assisted magnetron sputtering. *Plasma Sources Sci. Technol.* **2011**, *20*, 035013. [CrossRef]
51. Craig, S.; Harding, G.L. Effects of Argon Pressure and Substrate Temperature on the Structure and Properties of Sputtered Copper Films. *J. Vac. Sci. Technol.* **1981**, *19*, 205–215. [CrossRef]
52. Pinto, R.; Poothra, J.I.; Purandare, S.C.; Pai, S.P.; D'Souza, C.P.; Kumar, D.; Sharon, M. Growth and Microstructural Study of Radio Frequency Magnetron Sputtered MgO Films on Silicon. *J. Vac. Sci. Technol. A* **1991**, *9*, 2670–2674. [CrossRef]

Disclaimer/Publisher's Note: The statements, opinions and data contained in all publications are solely those of the individual author(s) and contributor(s) and not of MDPI and/or the editor(s). MDPI and/or the editor(s) disclaim responsibility for any injury to people or property resulting from any ideas, methods, instructions or products referred to in the content.